Effect of *n*-Alcohols on the Structure and Stability of the *Drosophila* Odorant Binding Protein LUSH[†]

Brigid K. Bucci,[‡] Schoen W. Kruse,[‡,§] Anna B. Thode, Sylvia M. Alvarado, and David N. M. Jones*

Department of Pharmacology and Program in Biomolecular Structure, University of Colorado at Denver and Health Sciences Center, 12801 East 17th Avenue M/S 8303, P.O. Box 6511, Aurora, Colorado 80045

Received August 19, 2005; Revised Manuscript Received November 9, 2005

ABSTRACT: LUSH is an odorant binding protein expressed in the olfactory organs of *Drosophila melanogaster* that is required for the detection of alcohol in adult flies. Here we demonstrate that, in the absence of ligand, in vitro LUSH exists in a partial molten globule state. The presence of short-chain *n*-alcohols at pharmacologically relevant concentrations less than 50 mM shifts the conformational equilibrium to a more compact state that exhibits reduced binding of the fluorescent dye 1-anilino-8-naphthalenesulfonic acid. Equilibrium unfolding studies of LUSH−alcohol complexes reveal that, for a series of short-chain *n*-alcohols, each methylene group can contribute approximately 1 K cal mol^{-1} to the overall stability of the protein−alcohol complex. Using NMR spectroscopy, we have identified the regions of LUSH that show increased conformational stability on binding alcohols. These residues primarily line the alcohol-binding pocket. The results presented here provide a direct measure of the degree of stability that alcohol imparts on LUSH. These observations may represent a model for how ethanol can stabilize alternative protein conformations in alcohol-sensitive human proteins and ultimately lead to the observed changes in higher order function throughout the central nervous system.

Alcohols dramatically affect the function of many cellular proteins and have a direct impact on a range of biological functions, including learning, memory, motor function, and metabolism. In humans, these effects are observed in the range of 5−50 mM, and the legal limit for driving in many U.S. states is a blood alcohol concentration of 0.08 mg %, which corresponds to ∼17 mM ethanol. In the central nervous system, alcohols affect the function of a number of ligand-gated ion channels (LGICs),[1] including *N*-methyl-D-aspartate (NMDA)-type glutamate receptors, γ-aminobutyric acid (GABA) receptors, nicotinic acetylcholine (nACh), and glycine receptors (Gly-R) (*1*−*3*). Changes in the activities of these receptors have been linked to intoxication, the development of dependency and tolerance, seizures during withdrawal (*4*), and fetal alcohol syndrome (*5*).

The potency of *n*-alcohols to modify ion-channel function is correlated with the hydrophobicity of the alcohol (*6*−*8*). However, ion channels often exhibit a "cutoff" phenomenon whereby increasing the length of the alcohol chain increases its potency to a point at which further increases in chain length have no additional effect on the receptor or, alternatively, fail to affect receptor function altogether (*9*−*11*). In some cases, this "cutoff" phenomenon may be related to the limiting solubility of the alcohols combined with the binding affinity for the alcohol (*12*). Yet, overall, there is now a large body of evidence that these LGICs contain a sterically restricted alcohol-binding site. Domain swap experiments to generate chimeric receptors can change the length of the alcohol that can affect receptor function (*13*), and single-point mutations can abolish or reduce alcohol sensitivity of the GABA and glycine receptors (*14*). More recently, cross-linking studies of specific cysteine mutants with alkyl methanethiosulfonate (MTS) reagents have shown that channel gating in response to ligand changes the accessibility of amino acids to alcohols and the size of the alcohol that can bind to the receptor (*15, 16*). Interestingly, in some cases, the use of longer chain MTS reagents can produce constitutively open ion channels (*16*). These studies led to the suggestion that alcohols bind in a water-filled pocket at the core of a four-helix bundle that forms the transmembrane domain of the receptor and that binding to this site stabilizes the open conformation of the receptor (*16*).

We are using the alcohol-sensitive odorant binding protein (OBP), LUSH, from *Drosophila melanogaster* (*17*) as a model system to investigate the biophysical nature of alcohol−protein interactions at alcohol concentrations that produce intoxication in humans. OBPs are essential components of the invertebrate olfactory system that mediate the behavioral response to odorant molecules, which provide signals for feeding, mating, and other social behaviors (*18*). LUSH was originally identified as responsible for mediating an avoidance response to short-chain *n*-alcohols (*17*), and this is associated with differential neuronal responses of T2B-type sensilla in *lush* null mutants compared to wild-type flies

[†] This work was supported by American Heart Association Predoctoral Fellowships to B.K.B. (0510005Z) and S.W.K. (0310065Z) and by NIH/NIAAA (AA013618) to D.N.M.J.

* Corresponding author. Tel.: (303) 724-3600. Fax: (303) 724-3663. E-mail: david.jones@uchsc.edu.

[‡] These authors contributed equally to this work.

[§] Present address: Laboratory of Structural Sciences, Van Andel Research Institute, 333 Bostwick Ave., Grand Rapids, MI 49503.

[1] Abbreviations: PBP, pheromone binding protein; OBP, odorant binding protein; NMR, nuclear magnetic resonance; CD, circular dichroism; ANS, 1-anilino-8-naphthalenesulfonic acid; LGIC, ligand-gated ion channel.

10.1021/bi0516576 CCC: $33.50
Published on Web 01/20/2006

(*19*). The exact function of OBPs is unclear, but previous work has suggested that OBPs may function to solubilize hydrophobic pheromone ligands (*20*−*24*), transport odorants for presentation to olfactory receptors (*23*, *25*−*27*), or clear the sensillum lymph of excess odorant (*18*, *28*, *29*). More recently, it has been suggested that a specific combination of OBP with a ligand is required to produce the appropriate conformational change that leads to activation of an odorant receptor (*30*−*34*). In support of this, Pophof showed that activation of odorant receptor neurons is enhanced by the formation of an OBP−odorant pair, and this activation is selective toward a specific odorant receptor (*35*, *36*). In contrast, other studies appear to require no specific involvement of OBPs for odorant receptor activation (*37*, *38*).

The structures of LUSH (*32*), as well as a number of other OBPs, have been solved at atomic resolution. These include the pheromone binding protein (PBP) from silkworm moth *Bombyx mori* (BmPBP) (*21*, *39*, *40*), the honeybee *Apis mellifera* (AmelPBP) (*41*), the cockroach *Leucophaea maderae* (LmaPBP) (*42*), and the giant silk moth *Antheraea polyphemus* (ApolPBP1) (*43*). The general structure of OBPs consists of six α-helices surrounding a hydrophobic ligand-binding pocket which differs in size and shape between each protein. All these OBPs have a set of six cysteines that form three conserved disulfide bonds. In the X-ray crystal structures of LUSH−alcohol complexes, we found that alcohol binds to a single site in the protein formed by a network of concerted hydrogen-bonding residues located at one end of the hydrophobic pocket (*32*). This binding site has some sequence and/or structural similarities to regions of several LGICs that have previously been implicated in inferring sensitivity to alcohol. We hypothesize that the alcohol-binding site in LUSH may represent a more general structural motif for functionally relevant alcohol-binding sites in proteins.

Here we present results that characterize the effects of *n*-alcohols on the structure and stability of LUSH. We show that, in the absence of ligand, LUSH exists in vitro in a partially unstructured state, and binding of alcohols shifts the solution conformation to a more compact folded state which is accompanied by an increase in the overall protein stability. We have identified those regions of the protein that show the largest changes in local dynamics on binding alcohol, and we have shown that these are predominantly associated with the residues that line the alcohol-binding pocket. Our results provide a quantitative measure of the ability of short-chain alcohols to stabilize protein structure at physiologically relevant concentrations. This information may help us to better understand how LUSH activates insect odorant receptors and also how alcohol can produce changes in protein structure that may directly lead to intoxication and ultimately alcohol dependency.

EXPERIMENTAL PROCEDURES

Protein Expression and Purification. The LUSH cDNA previously described (*32*) was subcloned into the pET-13a vector (*44*) between the *Nde*1 and *Bam*H1 restriction sites, and the resulting plasmid was transformed into *Escherichia coli* strain BL21 (DE3) (Novagen). The protein (124 amino acids) was expressed without any affinity tag and was isolated from inclusion bodies. Protein expression and refolding was performed as described previously (*32*) with the following additional steps. The protein was refolded with 1% v/v ethanol, and all subsequent buffers used contained 0.3% v/v ethanol. For protein purification, a 1 mL HiTrap DEAE fast-flow anion-exchange column (Amersham Biosciences) was used to remove excess DNA, and after concentration the protein was further purified by cation-exchange chromatography using POROS HS resin (Boehringer Mannheim) on an ÄKTA purifier system (Amersham Pharmacia Biotech). The protein eluted in approximately 150 mM NaCl in 20 mM sodium phosphate, pH 6.5. After exhaustive dialysis to remove salt, samples were concentrated in an Amicon stirred ultrafiltration cell with a YM3 (Millipore) membrane. The purified protein was analyzed by denaturing polyacrylamide gel electrophoresis (SDS−PAGE) and its identity confirmed using mass spectrometry.

Equilibrium Unfolding Studies. Ultrapure urea was purchased from ICN Biomedicals Inc., and reagent-grade sodium phosphate (NaH_2PO_4 and Na_2HPO_4) was from Fischer Scientific. A stock solution of urea (9 M) was prepared volumetrically at 25 °C in 20 mm sodium phosphate pH 6.5 (buffer A), and 24 different concentrations of urea (0−7.27 M) were made by diluting the stock urea solution with buffer A in volumetric flasks immersed in a water bath equilibrated at 20 °C. All buffers were filtered through a 0.22 μm filter, and stock solutions were frozen at −20 °C until use.

Purified protein was exhaustively dialyzed against buffer A to yield the apo-protein, and LUSH−alcohol complexes were prepared by dialysis into the same buffer containing 50 mM ethanol or *n*-butanol or 25 mM *n*-hexanol. Protein samples were concentrated individually to a final stock concentration of 102.4, 114.4, 110.4, and 105.3 μM for the apo-LUSH, ethanol, *n*-butanol, and *n*-hexanol complexes, respectively. Each sample was flash frozen in liquid nitrogen and stored at −20 °C until use. Immediately prior to each experiment, the appropriate *n*-alcohol was added to an aliquot of each of the 24 different urea concentrations to give a final concentration of 50 mM ethanol, 50 mM *n*-butanol, or 25 mM *n*-hexanol. Subsequently, 900 μL of each urea solution was mixed with 100 μL of the stock protein solution (with or without alcohol) to give final urea concentrations of 0−6.9 M in 0.33 M steps. Each sample was inverted five times and incubated at 25 °C for at least 1 h.

Fluorescence measurements were collected on a PTI LPS-220 (Photon Technology International) fluorimeter with a xenon lamp. Each sample was added to a stoppered stirred cuvette cell with a 4 × 10 mm (excitation × emission) path length (Hellma GmbH & Co.). Fluorescence experiments were performed at 25 °C with an excitation wavelength of 295 nm, and the emission was recorded in the range of 310−400 nm with an integration time of 1 s nm^{-1}. Each spectrum was the average of two scans. Baselines were corrected by subtraction of the spectrum of buffer alone or buffer with alcohol. Each experiment was performed independently three times.

Urea-dependent unfolding data were fit to a two-state model where the protein was assumed to be in either the folded state (N) or the unfolded state (U). The signals from the folded and unfolded states of the protein were assumed to be linearly dependent on urea concentration in order to fit the pre- and post-transition baselines (*45*). The linear extrapolation method was used to evaluate the free energy

for unfolding in the absence of denaturant ($\Delta G^{\circ}_{H_2O}$) (*45*) as shown in eq 1, where *m* is the urea-dependent change in fluorescence and the free energy of denaturation (ΔG_D) is expressed in the usual way (eq 2).

$$\Delta G_D = \Delta G^{\circ}_{H_2O} + m[\text{urea}] \quad (1)$$

$$\Delta G_D = -RT \ln K_{eq} \quad (2)$$

Values of $\Delta G^{\circ}_{H_2O}$ were determined by fitting the fluorescence intensity as a function of urea concentration to eq 3 (*45*) using the Levenberg−Marquardt algorithm in the program KaleidaGraph 3.51 (Synergy Software). y_N and y_U

$$Y = \frac{(y^{\circ}_N + m_N[\text{urea}]) + (y^{\circ}_U + m_U[\text{urea}])\exp[(-\Delta G^{\circ}_{H_2O} + m[\text{urea}])/RT]}{1 + \exp[(-\Delta G^{\circ}_{H_2O} + m[\text{urea}])/RT]} \quad (3)$$

represent the fluorescence contribution from the native and unfolded states, respectively, at a specific denaturant concentration; y°_N and y°_U are the values of the fluorescence extrapolated to 0 M denaturant; and m_N and m_U are the slopes of the pre- and post-transition regions, respectively (*45*). Results for individual complexes were analyzed using a one-way analysis of variance (ANOVA) test, and comparisons between measurements were determined using a Tukey post hoc analysis in Kaleidagraph.

Measurement of ANS Binding. Samples of LUSH were prepared as described above and diluted to a final protein concentration of 2 μM. 1-Anilino-8-naphthalenesulfonic acid (ANS) (Molecular Probes) was added to a final concentration of 26 μM and equilibrated for 30 min with stirring at 25 °C. Fluorescence experiments were performed on a Jobin-Yvon Fluorolog3 spectrometer at an excitation wavelength of 370 nm, with the emission detected over the range of 390−600 nm. Data were collected at 25 °C and at 0.5 nm intervals with a 1 s integration time and a slit width of 2 nm for both the excitation and emission monochromators. Data from two scans were averaged for each experiment, and three independent experiments were performed for each complex. Data were corrected by subtraction of the spectrum of buffer containing the appropriate alcohol. The concentration of stock solutions of ANS was calculated using an extinction coefficient of 7800 cm^{-1} M^{-1} at 372 nm (Molecular Probes Handbook). Solutions with alcohol contained 50 mM ethanol, 33 mM butanol, or 36 mM hexanol.

NMR Spectroscopy. For NMR spectroscopy, protein was isotopically labeled with ^{15}N and/or ^{13}C by overexpression from cells grown in minimal media containing ^{15}N-labeled ammonium chloride (99 atom %) and $^{13}C_6$-labeled glucose (98 atom %) (Spectra Gases) as the sole nitrogen and carbon sources, respectively. Samples were prepared in 20 mM sodium phosphate, pH 6.5 (buffer A), containing 30 mM ethanol, 33 mM butanol, 27 mM pentanol, or 36 mM hexanol. D_2O was added to a final concentration of 10% to give protein concentrations in the range of 400−600 μM. Samples without alcohol were prepared by exhaustive dialysis into buffer A without alcohol. All spectra were collected at 25 °C on Varian Inova spectrometers operating at a proton frequency of 500 or 600 MHz. Gradient-enhanced $^1H-^{15}N$ heteronuclear single-quantum correlation (HSQC) spectra (*46*) were acquired using Watergate suppression (*47*, *48*).

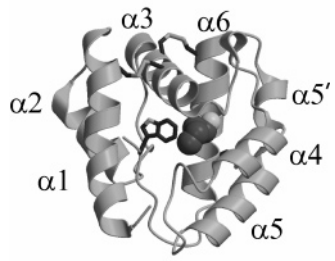

FIGURE 1: Ribbon diagram of LUSH showing location of the alcohol-binding site and Trp123. Trp123 is shown in thick black lines, and butanol is represented as a space-filling model. The diagram is based on the coordinates of the LUSH−butanol complex (RCSB accession code 1OOH) and was made using Molscript (*75*) and rendered using Raster3D (*76*).

Assignment of NMR Spectra. Backbone and side-chain assignments for $^{15}N/^{13}C$-labeled LUSH were determined at 25 °C using 3D NOESY−HSQC (*49*), HSQC−NOESY−HSQC (*50*), HNCACB (*51*), CBCA(CO)NH (*52*), (H)C(CO)NH−TOCSY (*53*), HNCACO (*54*), and HNCO (*55*, *56*) spectra. ^1H chemical shifts were referenced directly to 2,2-Dimethyl-2-silapentane-5-sulfonate sodium salt (DSS), and ^{13}C and ^{15}N chemical shifts were referenced indirectly from the ratio of the gyromagnetic ratios (*57*).

Chemical shift predictions for LUSH were performed using the coordinates of the LUSH−butanol complex (RCSB code 1OOH) (*32*). All crystallographic waters and cofactors were removed prior to the calculations. Chemical shift predictions were carried out using the SHIFTX server (http://redpoll.pharmacy.ualberta.ca/shiftx/) (*58*) and SHIFTS (http://www.scripps.edu/mb/case/qshifts/qshifts.htm) (*59*, *60*).

RESULTS

Effect of Alcohol Chain Length on Urea-Induced Equilibrium Unfolding of LUSH. LUSH is highly sensitive to alcohol concentrations in the range of 25−50 mM, which are comparable to those that produce intoxication in humans. We have found that alcohol is absolutely required as a cofactor to refold protein from inclusion bodies, as judged by circular dichroism and NMR spectroscopy (Supporting Information Figure S1). Protein refolded in the absence of alcohol appears to be misfolded and/or relatively unstructured and is not affected by the addition of alcohol. In contrast, protein refolded with alcohol can be dialyzed to remove the alcohol or to replace it with other alcohols, and conformational changes are readily observed (see below).

The single tryptophan (Trp123) in LUSH is the penultimate residue in the C-terminal strand of the protein, which folds back into the core of the protein to form one edge of the alcohol-binding pocket (Figure 1) (*32*). The fluorescence emission spectrum of LUSH shows both an increase in the fluorescence intensity and a red shift in the wavelength of the emission maximum upon addition of 8 M urea (Figure 2). These changes indicate that the intrinsic fluorescence of Trp123 is significantly quenched in the native state, and this is most likely due to the close proximity (within 5 Å) of three phenylalanine residues (Phe36, Phe113, and Phe121) (*61*). These large spectroscopic changes allowed us to use fluorescence to probe the effect of alcohols on the conformational stability of LUSH.

Urea-induced unfolding of LUSH occurs in an apparent two-state process with no observable intermediates. Free

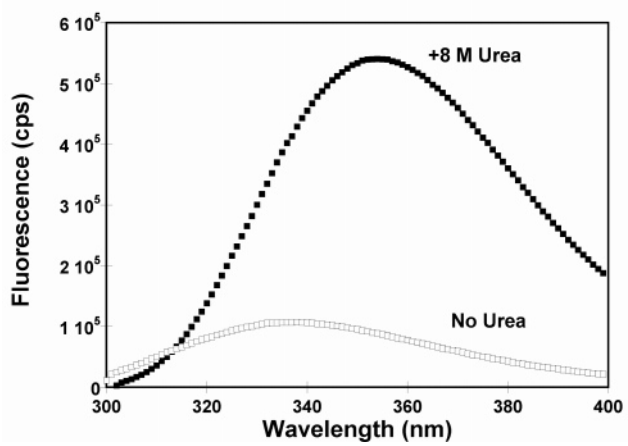

FIGURE 2: Tryptophan fluorescence emission spectra of LUSH. Intrinsic tryptophan emission of the LUSH−ethanol complex recorded at 25 °C in 20 mM sodium phosphate at pH 6.5 (○) and in the same buffer in the presence of 8 M urea (■). The protein concentration was 20 μM.

Table 1: Results of Urea-Dependent Unfolding of LUSH

protein complex	$[urea]_{mid}$ (M)[a]	$\Delta G^{\circ}_{H_2O}$ (kcal mol^{-1})[a]	*m* value (kcal mol^{-1} M^{-1})[a]	$\Delta\Delta G^{\circ}_{H_2O}$ (kcal mol^{-1})[b]
apo-LUSH	2.39 ± 0.04	3.02 ± 0.21	1.24 ± 0.06	
LUSH−ethanol	2.62 ± 0.05	3.41 ± 0.45	1.27 ± 0.16	0.41
LUSH−*n*-butanol	2.98 ± 0.08	5.26 ± 0.27	1.76 ± 0.13	1.85
LUSH−*n*-hexanol	4.11 ± 0.05	7.35 ± 0.20	1.77 ± 0.03	2.09

[a] Reported values are the average of three separate measurements for each complex, and the error is reported as ± the standard deviation. [b] The value of $\Delta\Delta G^{\circ}_{H_2O}$ is the difference in $\Delta G^{\circ}_{H_2O}$ for each complex compared to the complex immediately above it in this table.

energies of unfolding in the absence of denaturant, $\Delta G^{\circ}_{H_2O}$, and the urea dependence of unfolding, the *m* value (Table 1), for a series of LUSH−alcohol complexes were obtained using the linear extrapolation method (*62*) (eq 3) and revealed that extending the length of the alcohol chain leads to a significant increase in the overall stability of the complex. While we found no statistical difference in the value of $\Delta G^{\circ}_{H_2O}$ between the free protein and the ethanol complex, values of $\Delta G^{\circ}_{H_2O}$ between the three individual LUSH−alcohol complexes analyzed in the same way are significantly different, with $p < 0.0005$ in all cases. A plot of $\Delta G^{\circ}_{H_2O}$ as a function of the alcohol chain length (Figure 3B) reveals that this increase in stability is linearly dependent on the number of carbon atoms in the alkyl chain and that each additional methylene group contributes 0.98 ± 0.03 kcal mol^{-1} ($R > 0.999$) to the overall stability. This linear dependence correlates well with the established relationships for the chain-length dependence of alcohol potency (*6*, *7*, *63*, *64*) and binding constants to voltage-gated potassium channels for small-chain *n*-alcohols (*65*).

In urea-dependent unfolding studies, *m* values are most closely correlated with differences in the solvent-accessible surface area (SASA) between the folded and unfolded states of the protein (*66*, *67*). The *m* value determined for apo-LUSH is not significantly different from that for the LUSH−ethanol complex. Additionally, there is no significant difference between the values obtained for the LUSH−butanol complex and the LUSH−hexanol complex. However, *m* values for the butanol and hexanol complexes are significantly different ($p < 0.005$) when compared to those of the

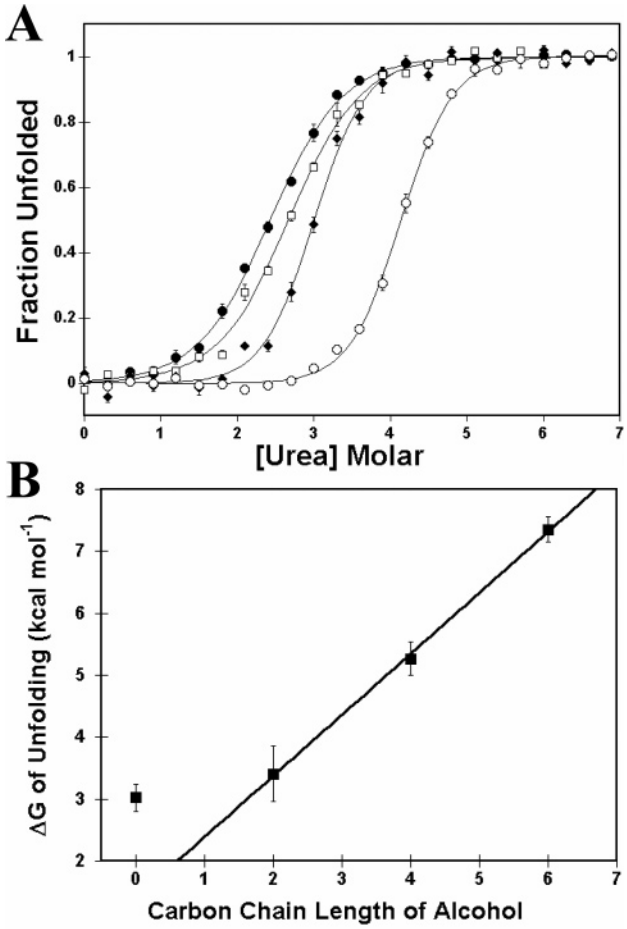

FIGURE 3: Effect of *n*-alcohols on the urea-dependent unfolding of LUSH. (A) Plot of the fraction of unfolded protein as a function of urea concentration determined using the values reported in Table 1: apo-LUSH (●), LUSH−ethanol complex (□), LUSH−butanol (◆), and LUSH−hexanol (○). Error bars are ± standard deviation for each point. **(**B**)** Plot of values of $\Delta G^{\circ}_{H_2O}$ as a function of alcohol chain length. The line drawn was fit to values of $\Delta G^{\circ}_{H_2O}$ for the three LUSH−alcohol complexes. Error bars are ± standard deviation for each point.

apo-protein and ethanol complexes. This indicates that unfolding of either the butanol or hexanol complex is associated with a greater change in the SASA compared to unfolding of either the ethanol complex or the apo-protein.

ANS Fluorescence Studies with LUSH−Alcohol Complexes. Binding of ANS to proteins is routinely used as a probe for the presence of partially folded or molten globule states of proteins (*68*, *69*). The fluorescence emission spectrum of ANS recorded in the presence of apo-LUSH compared to that of ANS alone shows a large increase in the emission intensity, accompanied by a blue-shift in the emission maximum to 456 nm, indicative of ANS binding to exposed hydrophobic surfaces in the protein (Figure 4). In contrast, the spectra of ANS in the presence of the LUSH−alcohol complexes show significantly reduced signal intensity and a progressive shift of the emission maxima to longer wavelengths, and this is dependent on the chain length of the alcohol (Figure 4). This result supports the urea-unfolding experiments and confirms that binding of alcohols progressively stabilizes the native state of the protein in a chain-length-dependent fashion. These data further suggest that apo-LUSH is a partially natively unfolded protein that resemble a molten globule state, and binding alcohols

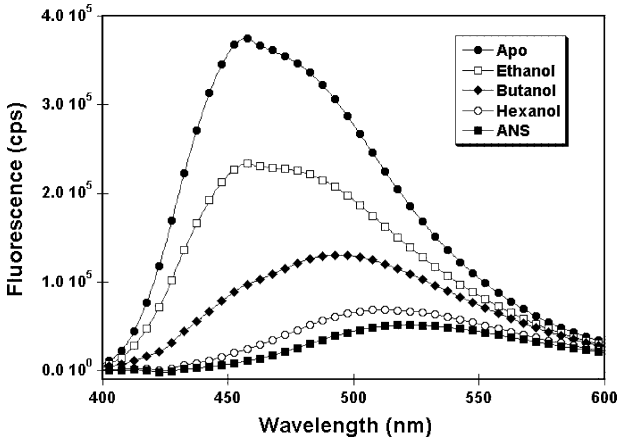

FIGURE 4: Fluorescence emission spectra of ANS binding to LUSH−alcohol complexes. Emission spectra of 26 μM ANS recorded in the presence of apo-LUSH (●), LUSH−ethanol (□), LUSH−butanol (◆), and LUSH−hexanol (○). In each case the protein concentration was 2 μM. The spectrum of ANS alone in buffer is also shown (■). The addition of alcohol has no effect on the emission spectra of ANS on its own. Spectra were recorded in 20 mM sodium phosphate buffer at pH 6.5 and at 25 °C with an excitation wavelength of 370 nm. Each trace is the average of three independent experiments, and the error in the measurement is approximately the size of the symbols used for each curve.

produces a more compact state of the protein. This is intriguing, as *n*-alcohols generally unfold proteins (*70*); however, this typically occurs at concentrations in the 5−50% range (1−8 M ethanol). Some exceptions include bovine serum albumin (*12*, *71*), which is stabilized by alcohols in the millimolar range. In contrast, alcohol destabilizes myoglobin in the same concentration range (*12*).

Identification of Amino Acids Stabilized by Binding of Alcohols. Urea unfolding and ANS binding are consistent with our previous NMR studies which show that, in the absence of alcohol, a significant part of the protein is in conformational exchange on the NMR time scale (*32*). This is manifested as either severely broadened or missing peaks in the ^{1}H−^{15}N HSQC spectrum. In the spectrum of the apoprotein, we observe only 40 well-resolved, sharp peaks from the backbone amide groups out of a possible 118 (Figure 5A). In contrast, we observe 73 peaks in the spectrum of the LUSH−ethanol complex and 107 peaks in the spectrum of the LUSH−butanol complex (*32*). NMR spectra recorded in the presence of hexanol show a continued improvement in quality, such that 112 peaks are now observable (Figure 5B).

To better understand how physiologically relevant concentrations of short-chain *n*-alcohols can stabilize protein structures, we have initiated a solution NMR study of LUSH. Sequence-specific chemical shift assignments for the backbone and side-chain ^{1}H, ^{15}N, and ^{13}C resonances of LUSH were obtained using established three-dimensional triple-resonance NMR experiments (see Experimental Procedures) on ^{15}N- and ^{13}C-labeled LUSH in the complexes it forms with 1-butanol, 1-pentanol, and 1-hexanol. These assignments are 94% complete (Supporting Information Table S1). Several residues could not be assigned because of the exchange broadening that remains even in the spectrum of the LUSH−hexanol complex. To assess if the structures of the LUSH−alcohol complexes are the same in solution and in the crystal, we compared the observed backbone ^{15}N and ^{13}C chemical shifts to values predicted from the crystal structure (RCSB accession code 1OOH) using the programs SHIFTX (*58*) and SHIFTS (*59*). In both cases, excellent correlations are observed between the observed and predicted shifts for the ^{13}Cα and ^{13}Cβ carbons, with $R = 0.964$ and 0.949 for Cα and 0.990 and 0.989 for Cβ using SHIFTX and SHIFTS, respectively (Supporting Information Figure S2). Analysis of the chemical shifts using the chemical shift index method (*72*) are also consistent with the α-helical regions defined in the crystal structure being maintained in solution (data not shown).

Regions of the protein that are unaffected by the binding of alcohol give rise to sharp peaks in all spectra (blue in Figure 6A). These residues cluster predominantly on the face

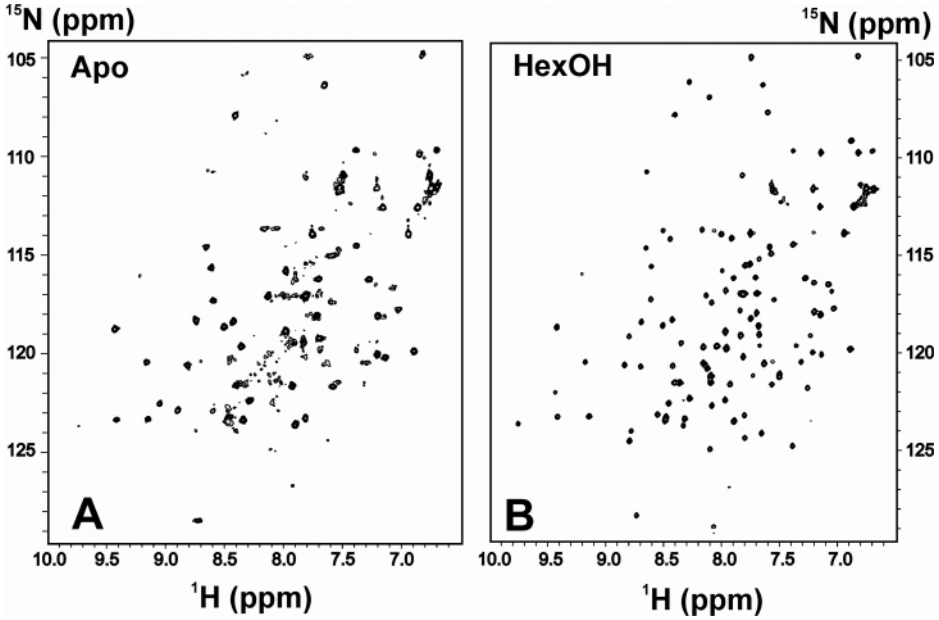

FIGURE 5: Effect of alcohol on the NMR spectrum of LUSH. ^{1}H−^{15}N HSQC spectrum of (A) apo-LUSH and (B) LUSH−hexanol complexes. Spectra were recorded at 25 °C in 20 mM sodium phosphate buffer at pH 6.5. The hexanol complex was prepared by dialysis of apo-LUSH into the same buffer containing 36 mM *n*-hexanol.

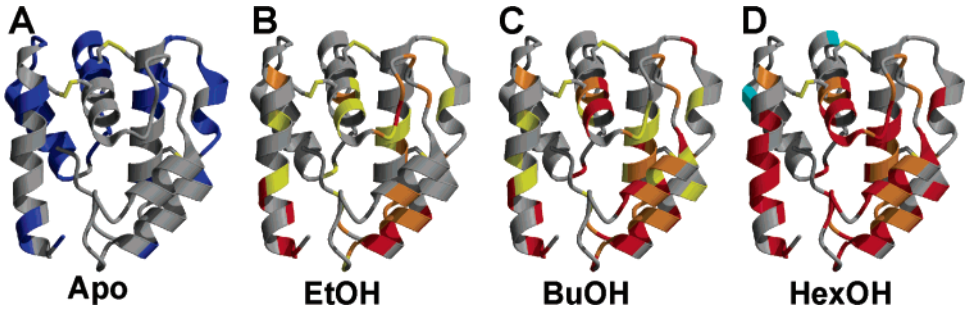

FIGURE 6: Location of residues in LUSH that are sensitive to alcohol binding. Residues that are unaffected by binding of alcohols (A) are shown in blue on a ribbon diagram of the LUSH−butanol complex (RCSB code 100H). Residues that show significant changes on binding ethanol **(**B**)**, butanol **(**C**)**, and hexanol **(**D**)**. The magnitude of the changes is indicated by color: yellow for small changes, orange for medium changes, and red for the strongest changes.

of the protein that contains α-helix2 (α2) and α-helix6 (α6) and are located near the N-terminus of α1, in the loop between α1 and α2, in α2, in the loop connecting α2 to α3, at the N-terminal end of α3, in the stretch of 3_{10}-helix (α5′), and at the N-terminal end of α6. In contrast, amino acids that show a significant improvement in line width in the LUSH−ethanol complex are located predominantly on the opposite face of the protein (Figure 6B): in α1, in the loop connecting α3 to α4, at the C-terminal end of α4, in α5, at the C-terminal end of α6, and in the loop that connects α6 to the C-terminal extended strand. A number of these residues form part of the alcohol-binding pocket or directly contact residues within the pocket, including Thr-48 and Gly-56 to Asn-59. The alcohol-binding site is formed predominantly by Thr-48, Ser-52, and Thr-57 (*32*). Unfortunately, the peak from Ser-52 is only completely resolved in the spectrum of the LUSH−hexanol complex, and so we cannot classify changes in line width for this residue. However, the observation that the backbone amides of Thr-48 and Thr-57 show improvements in line widths strongly suggests that this region of the protein is stabilized by binding of alcohol. At this stage, we cannot rule out the possibility that the observed differences in exchange broadening for these residues is a result of changes in the local dynamics of aromatic amino acids in this region rather than a result of a direct stabilization of the protein main chain.

Changes in the NMR spectrum recorded in the presence of butanol occur in the same regions of the protein as observed with ethanol (Figure 6C). However, the magnitudes of the changes are larger and occur for a greater number of amino acids in these regions. For example, an increased number of changes are observed in α4, and the changes in the center of α3 now include residues 48−51. The changes in stability induced by pentanol and hexanol follow the same trend as butanol, with even more residues showing improvements in line widths (Figure 6D). Interestingly, peaks from residues Thr-25 and Arg-42 are observed in all spectra except those from the pentanol and hexanol complexes, in which they are very weak (cyan in Figure 6D). This observation is intriguing, as *lush* null flies fail to show a difference in their behavioral response to alcohols longer than butanol (*17*). This may indicate that regions of the protein destabilized by alcohols longer than butanol are somehow involved in activating odorant receptors in response to short-chain *n*-alcohols. However, as these residues are found at the N-terminus of α2 and α3, respectively, and are in regions of the protein that are otherwise unchanged on binding alcohol, the exact implication of this observation is unclear at this point and requires further investigation.

DISCUSSION

LUSH is a unique odorant binding protein in that it modulates the activity of two very different odorant signals in two different sets of trichoid sensilla of *Drosophila*. LUSH is required for vaccenyl acetate-dependent activation of T1 sensilla and alcohol-dependent inhibition of type T2B sensilla (*19*). T1-type sensilla that express LUSH also exhibit spontaneous depolarizations approximately every second, which are completely abolished in *lush* null flies but can be recovered in *lush* rescue mutations or through the use of recombinant protein (*19*). This recovery appears to be specific for LUSH, as expression or use of other OBPs or unfolded LUSH fails to recover this activity. The implication is that the protein exists in a dynamic conformational exchange and occasionally samples a conformation that is capable of activating odorant receptor neurons.

The results presented here provide further insight into the nature of the conformational state of LUSH that exists in the sensilla lymph in the absence of ligand. It appears that LUSH is a natively unstable protein and in vitro exists in a partially unfolded or molten globule state. Binding of ligand leads to an increase in overall stability of the protein and a shift to a more compact state of the protein. This is reflected in higher concentrations of urea required to induce unfolding, dramatic improvements in the appearance of the NMR spectrum of the complexes, and decreased binding of the fluorescent dye ANS. For alcohols, the increase in protein stability is linearly dependent on the chain length of the alcohol, which is interesting as in vivo butanol is more effective at inhibiting type T2B sensilla than ethanol (*19*). The fact that purified, recombinant protein is able to recapitulate the activity of endogenously expressed protein in *lush* null flies (*19*) indicates that the conformation of the protein in vivo is likely to be the same as that seen in vitro. To date, we have only examined the binding of alcohols with up to six carbons, and it is likely that larger ligands, such as vaccenyl acetate, are able to produce an even greater increase in the overall stability of the protein. However, this increased stability is not the only factor that is likely to govern the in vivo response, as other groups have shown that odorant-invoked responses depends on the identity of the receptor expressed in the odorant receptor neuron (*37*). The precise response elicited by an odorant molecule will most probably depend on its ability to stabilize the "functional" state of

the OBP, combined with the spatial distribution of the specific odorant receptor or other accessory proteins (*19*).

Ligand binding has been shown to produce conformational changes in a number of other insect OBPs, including ApolPBPs 1−3 and LmaPBP (*42*), and in the chemosensory protein from *Mamestra brassicae* (*73*). Additionally, pH-dependent conformational changes have been reported for the BmPBP (*20*, *39*) and for an OBP from the honeybee, *A. mellifera* (*74*). For BmPBP it was shown that changes in pH lead to a dramatic shift in the conformation of the C-terminal tail. At higher pH values, this tail is located on the outside of the protein in an extended conformation, but at pH < 5.5 the tail adopts an α-helical conformation, folds into the core of the protein, and occupies the ligand-binding site. This led to the hypothesis that changes in the pH produced by close approach of the OBP to membranes may act as a mechanism to control ligand binding and release, which ultimately leads to activation of odorant receptor neurons (*20*).

Conformational changes in the C-terminal tail of LUSH have previously been investigated using the fluorescent probe *N*-phenyl-1-naphthylamine (1-NPN) (*33*). In those studies, no changes in the intrinsic tryptophan fluorescence could be observed on binding of 1-NPN, which led to the suggestion that binding of ligands may cause the C-terminal tail to flip out into solution (*33*). Our unfolding studies argue against such a conformational change, which we observe leads to an increase in tryptophan fluorescence. Rather, our results support the alternative explanations put forward that Trp-123 either is not accessible to 1-NPN or does not form part of the 1-NPN-binding site (*33*). An alternative explanation is that the intrinsic fluorescence of the single tryptophan in LUSH is already highly quenched in the unbound state by virtue of the close proximity of three phenylalanines.

The chain-length-dependent, alcohol-induced structural stability in LUSH correlates well with the chain-length dependency of alcohol potency observed for a number of ion channels that are thought to be primary targets of alcohols in the central nervous system (*6*, *7*, *63*, *64*). For example, in studies of the *Drosophila* Shaw2 K^+ voltage-sensitive channel, extending the length of the alkyl chain in C2, C4, and C6 *n*-alcohols produced a linear change in the free energy of binding by ∼0.8 K cal mol^{-1} per methylene group, and this correlated with a linear change in the extent of channel inhibition (*65*). Studies of the glycine receptor show that the size of the binding pocket for alcohols and anesthetics is dependent on conformational changes in response to ligand and that binding of ligand can stabilize the open state of the receptor (*16*). Our results provide insight into the degree of conformational stability that alcohol can infer to proteins by binding to a single site and further support the hypothesis that alcohols act to modulate function by preferentially stabilizing one conformation of the protein.

ACKNOWLEDGMENT

We thank Drs. Carlos Catalano and Karl Maluf for access to and advice in using their fluorescence spectrometer, Drs. Robert Hodges and Brian Trippet for mass spectrometric analysis and stimulating discussion on data analysis, and Dr. Brian Hoover for assistance in data analysis. X-ray crystallography facilities and NMR spectrometers were purchased with funds provided by the Howard Hughes Medical Institute and the University of Colorado Comprehensive Cancer Center, and their operation is supported by the University of Colorado Cancer Center Core Grant and the Program in Biomolecular Structure.

SUPPORTING INFORMATION AVAILABLE

Figures illustrating the effect of alcohol on protein refolding as measured by CD and NMR, calculations comparing the observed and predicted NMR chemical shifts, and a list of chemical shift assignments. This material is available free of charge via the Internet at http://pubs.acs.org.

REFERENCES

1. Woodward, J. J. (1999) Ionotropic glutamate receptors as sites of action for ethanol in the brain, *Neurochem. Int. 35*, 107−113.
2. Lovinger, D. M. (1997) Alcohols and neurotransmitter gated ion channels: Past, present and future, *Naunyn-Schmiedeberg's Arch. Pharmacol. 356*, 267−282.
3. Harris, R. A. (1999) Ethanol actions on multiple ion channels: Which are important? *Alcohol. Clin. Exp. Res. 23*, 1563−1570.
4. Faingold, C. L., N'Gouemo, P., and Riaz, A. (1998) Ethanol and neurotransmitter interactions—from molecular to integrative effects, *Prog. Neurobiol. 55*, 509−535.
5. Ikonomidou, C., Bittigau, P., Ishimaru, M. J., Wozniak, D. F., Koch, C., Genz, K., Price, M. T., Stefovska, V., Horster, F., Tenkova, T., Dikranian, K., and Olney, J. W. (2000) Ethanol-induced apoptotic neurodegeneration and fetal alcohol syndrome, *Science 287*, 1056−1060.
6. Overton, E. (1896) Uber die osmotischem eigenschaften der zell in ihrer betdeuttung dur die toxikologie und pharmakologie, *Z. Phys. Chem. 22*, 189−209.
7. Meyer, H. (1901) Zur theorie der alkolnarkose der einfluss wechselnder der temperatur auf wirkungsstarke und theilungscoefficient der narcotica, *Naunyn-Schmeideberg's Arch. Exp. Pathol. Pharmacol. 46*, 338−346.
8. Janoff, A. S., Pringle, M. J., and Miller, K. W. (1981) Correlation of General Anesthetic Potency With Solubility in Membranes, *Biochim. Biophys. Acta 649*, 125−128.
9. McCreery, M. J., and Hunt, W. A. (1978) Physicochemical Correlates of Alcohol Intoxication, *Neuropharmacology 17*, 451−461.
10. Lyon, R. C., McComb, J. A., Schreurs, J., and Goldstein, D. B. (1981) A Relationship Between Alcohol-Intoxication and the Disordering of Brain Membranes By a Series of Short-Chain Alcohols, *J. Pharmacol. Exp. Ther. 218*, 669−675.
11. Alifimoff, J. K., Firestone, L. L., and Miller, K. W. (1989) Anesthetic Potencies of Primary Alkanols—Implications For the Molecular Dimensions of the Anesthetic Site, *Br. J. Pharmacol. 96*, 9−16.
12. Eckenhoff, R. G., Tanner, J. W., and Johansson, J. S. (1999) Steric hindrance is not required for n-alkanol cutoff in soluble proteins, *Mol. Pharmacol. 56*, 414−418.
13. Mihic, S. J., Ye, Q., Wick, M. J., Koltchine, V. V., Krasowski, M. A., Finn, S. E., Mascia, M. P., Valenzuela, C. F., Hanson, K. K., Greenblatt, E. P., Harris, R. A., and Harrison, N. L. (1997) Sites of alcohol and volatile anesthetic action on GABA(A) and glycine receptors, *Nature 389*, 385−389.
14. Wick, M., Mihic, S., Ueno, S., Mascia, M., Trudell, J. R., Brozowski, S., Ye, Q., Harrison, N., and Harris, R. (1998) Mutations of gamma-aminobutyric acid and glycine receptors change alcohol cutoff: Evidence for an alcohol receptor? *Proc. Natl. Acad. Sci. U.S.A. 95*, 6504−6509.
15. Mascia, M. P., Trudell, J. R., and Harris, R. A. (2000) Specific binding sites for alcohols and anesthetics on ligand- gated ion channels, *Proc. Natl. Acad. Sci. U.S.A. 97*, 9305−9310.
16. Lobo, I. A., Mascia, M. P., Trudell, J. R., and Harris, R. A. (2004) Channel gating of the glycine receptor changes accessibility to residues implicated in receptor potentiation by alcohols and anesthetics, *J. Biol. Chem. 279*, 33919−33927.
17. Kim, M.-S., Repp, A., and Smith, D. P. (1998) LUSH Odorant-binding protein mediates chemosensory responses to alcohols in *Drosophila melanogaster*, *Genetics 150*, 711−721.

18. Vogt, R. G., and Riddiford, L. M. (1981) Pheromone binding and inactivation by moth antennae, *Nature 293*, 161−163.
19. Xu, P., Atkinson, R., Jones, D. N. M., and Smith, D. P. (2005) Drosophila OBP LUSH is Required for Activity of Pheromone-Sensitive Neurons, *Neuron 45*, 193−200.
20. Wojtasek, H., and Leal, W. (1999) Conformational change in the pheromone-binding portein from *Bombyx mori* induced by pH and by interaction with membranes, *J. Biol. Chem. 274*, 30950−30956.
21. Sandler, B. H., Nikonova, L., Leal, W. S., and Clardy, J. (2000) Sexual attraction in the silkworm moth: structure of the pheromone-binding-protein-bombykol complex, *Chem. Biol. 7*, 143−151.
22. Vogt, R. G., Riddiford, L. M., and Prestwich, G. D. (1985) Kinetic properties of a sex pheromone-degrading enzyme: the sensillar esterase of Antheraea polyphemus, *Proc. Natl. Acad. Sci. U.S.A. 82*, 8827−8831.
23. Kaissling, K. E. (1986) Chemo-electrical transduction in insect olfactory receptors, *Annu. Rev. Neurosci. 9*, 121−145.
24. Berg, M. J. V. d., and Ziegelberger, G. (1991) On the function of the pheromone binding protein in the olfactory hairs of *Antheraea polyphemus*, *J. Insect Physiol. 37*, 79−85.
25. Kaissling, K. E. (2001) Olfactory perireceptor and receptor events in moths: a kinetic model, *Chem. Senses 26*, 125−150.
26. Du, G., and Prestwich, G. D. (1995) Protein structure encodes the ligand binding specificity in pheromone binding proteins, *Biochemistry 34*, 8726−8732.
27. Krieger, J., and Breer, H. (1999) Olfactory reception in invertebrates, *Science 286*, 720−723.
28. Steinbrecht, R. A., and Muller, B. (1971) On the stimulus conducting structures in insect olfactory receptors, *Z. Zellforsch. Mikrosk. Anat. 117*, 570−575.
29. Ziegelberger, G. (1995) Redox-Shift of the Pheromone-Binding Protein in the Silkmoth Antheraea-Polyphemus, *Eur. J. Biochem. 232*, 706−711.
30. Tegoni, M., Campanacci, V., and Cambillau, C. (2004) Structural aspects of sexual attraction and chemical communication in insects, *Trends Biochem. Sci. 29*, 257−264.
31. Campanacci, V., Krieger, J., Bette, S., Sturgis, J. N., Lartigue, A., Cambillau, C., Breer, H., and Tegoni, M. (2001) Revisiting the specificity of *Mamestra brassicae* and *Antheraea polyphemus* pheromone-binding proteins with a fluorescence binding assay, *J. Biol. Chem. 276*, 20078−20084.
32. Kruse, S. W., Zhao, R., Smith, D. P., and Jones, D. N. (2003) Structure of a specific alcohol-binding site defined by the odorant binding protein LUSH from Drosophila melanogaster, *Nat. Struct. Biol. 10*, 694−700.
33. Zhou, J. J., Zhang, G. A., Huang, W., Birkett, M. A., Field, L. M., Pickett, J. A., and Pelosi, P. (2004) Revisiting the odorant-binding protein LUSH of Drosophila melanogaster: evidence for odour recognition and discrimination, *FEBS Lett. 558*, 23−26.
34. Riviere, S., Lartigue, A., Quennedey, B., Campanacci, V., Farine, J. P., Tegoni, M., Cambillau, C., and Brossut, R. (2003) A pheromone-binding protein from the cockroach Leucophaea maderae: cloning, expression and pheromone binding, *Biochem. J. 371*, 573−579.
35. Pophof, B. (2002) Moth pheromone binding proteins contribute to the excitation of olfactory receptor cells, *Naturwissenschaften 89*, 515−518.
36. Pophof, B. (2004) Pheromone-binding proteins contribute to the activation of olfactory receptor neurons in the silkmoths antheraea polyphemus and Bombyx mori, *Chem. Senses 29*, 117−125.
37. Hallem, E. A., Ho, M. G., and Carlson, J. R. (2004) The molecular basis of odor coding in the Drosophila antenna, *Cell 117*, 965−979.
38. Hallem, E. A., and Carlson, J. R. (2004) The odor coding system of Drosophila, *Trends Genet. 20*, 453−459.
39. Horst, R., Damberger, F., Luginbuhl, P., Guntert, P., Peng, G., Nikonova, L., Leal, W. S., and Wuthrich, K. (2001) NMR structure reveals intramolecular regulation mechanism for pheromone binding and release, *Proc. Natl. Acad. Sci. U.S.A. 98*, 14374−14379.
40. Lee, D., Damberger, F. F., Peng, G. H., Horst, R., Guntert, P., Nikonova, L., Leal, W. S., and Wuthrich, K. (2002) NMR structure of the unliganded Bombyx mori pheromone-binding protein at physiological pH, *FEBS Lett. 531*, 314−318.
41. Lartigue, A., Gruez, A., Briand, L., Blon, F., Bezirard, V., Walsh, M., Pernollet, J. C., Tegoni, M., and Cambillau, C. (2004) Sulfur single-wavelength anomalous diffraction crystal structure of a pheromone-binding protein from the honeybee Apis mellifera L, *J. Biol. Chem. 279*, 4459−4464.
42. Lartigue, A., Gruez, A., Spinelli, S., Riviere, S., Brossut, R., Tegoni, M., and Cambillau, C. (2003) The crystal structure of a cockroach pheromone-binding protein suggests a new ligand binding and release mechanism, *J. Biol. Chem. 278*, 30213−30218.
43. Mohanty, S., Zubkov, S., and Gronenborn, A. M. (2004) The solution NMR structure of Antheraea polyphemus PBP provides new insight into pheromone recognition by pheromone-binding proteins, *J. Mol. Biol. 337*, 443−451.
44. Gerchman, S. E., Graziano, V., and Ramakrishnan, V. (1994) Expression of chicken linker histones in *Escherichia coli*—sources of problems and methods for overcoming some of the difficulties, *Protein Express. Purif. 5*, 242−251.
45. Santoro, M. M., and Bolen, D. W. (1988) Unfolding free energy changes determined by the linear extrapolation method. 1. Unfolding of phenylmethanesulfonyl alpha-chymotrypsin using different denaturants, *Biochemistry 27*, 8063−8068.
46. Bodenhausen, G., and Ruben, D. J. (1980) Natural Abundance N-15 NMR By Enhanced Heteronuclear Spectroscopy, *Chem. Phys. Lett. 69*, 185−189.
47. Sklenar, V., Piotto, M., Leppik, R., and Saudek, V. (1993) Gradient-Tailored Water Suppression for H-1-N-15 Hsqc Experiments Optimized to Retain Full Sensitivity, *J. Magn. Reson. Ser. A 102*, 241−245.
48. Piotto, M., Saudek, V., and Sklenar, V. (1992) Gradient-Tailored Excitation for Single-Quantum Nmr-Spectroscopy of Aqueous-Solutions, *J. Biomol. NMR 2*, 661−665.
49. Marion, D., Driscoll, P. C., Kay, L. E., Wingfield, P. T., Bax, A., Gronenborn, A. M., and Clore, G. M. (1989) Overcoming the Overlap Problem in the Assignment of H-1-NMR Spectra of Larger Proteins By Use of 3-Dimensional Heteronuclear H-1-N-15 Hartmann−Hahn Multiple Quantum Coherence and Nuclear Overhauser Multiple Quantum Coherence Spectroscopy—Application to Interleukin-1-Beta, *Biochemistry 28*, 6150−6156.
50. Frenkiel, T., Bauer, C., Carr, M. D., Birdsall, B., and Feeney, J. (1990) HMQC−NOESY−HQMC, a three-dimensional NMR experiment which allows detection of nuclear Overhauser effects between protons with overlapping signals, *J. Magn. Reson. 90*, 420−425.
51. Wittekind, M., and Mueller, L. (1993) HNCACB, a High-Sensitivity 3D NMR Experiment to Correlate Amide-Proton and Nitrogen Resonances With the Alpha-Carbon and Beta-Carbon Resonances in Proteins, *J. Magn. Reson. Ser. B 101*, 201−205.
52. Grzesiek, S., and Bax, A. (1993) Amino-Acid Type Determination in the Sequential Assignment Procedure of Uniformly C-13/N-15-Enriched Proteins, *J. Biomol. NMR 3*, 185−204.
53. Lyons, B. A., and Montelione, G. T. (1993) An HCCNH Triple-Resonance Experiment Using C-13 Isotropic Mixing For Correlating Backbone Amide and Side-Chain Aliphatic Resonances in Isotopically Enriched Proteins, *J. Magn. Reson. Ser. B 101*, 206−209.
54. Bazzo, R., Cicero, D. O., and Barbato, G. (1996) A new three-dimensional pulse sequence for correlating intraresidue NH, N, and CO chemical shifts in C-13, N-15-labeled proteins, *J. Magn. Reson. Ser. B 110*, 65−68.
55. Kay, L. E., Ikura, M., Tschudin, R., and Bax, A. (1990) Three-dimensional triple-resonance NMR spectroscopy of isotopically enriched proteins, *J. Magn. Reson. 89*, 496−514.
56. Grzesiek, S., and Bax, A. (1992) Improved 3D Triple-Resonance NMR Techniques Applied to a 31-KDa Protein, *J. Magn. Reson. 96*, 432−440.
57. Markley, J. L., Bax, A., Arata, Y., Hilbers, C. W., Kaptein, R., Sykes, B. D., Wright, P. E., and Wuthrich, K. (1998) Recommendations for the presentation of NMR structures of proteins and nucleic acids (IUPAC Recommendations 1998), *Pure Appl. Chem. 70*, 117−142.
58. Neal, S., Nip, A. M., Zhang, H. Y., and Wishart, D. S. (2003) Rapid and accurate calculation of protein H-1, C-13 and N-15 chemical shifts, *J. Biomol. NMR 26*, 215−240.
59. Xu, X. P., and Case, D. A. (2001) Automated prediction of N-15, C-13(alpha), C-13(beta) and C-13′ chemical shifts in proteins using a density functional database, *J. Biomol. NMR 21*, 321−333.
60. Xu, X. P., and Case, D. A. (2002) Probing multiple effects on 15N, 13C alpha, 13C beta, and 13C′ chemical shifts in peptides using density functional theory, *Biopolymers 65*, 408−423.
61. Lakowicz, J. (1999) *Principles of Fluorescence Spectroscopy*, 2nd ed., Plenum Publishing Corp., New York.

62. Pace, C. (1986) Determination and analysis of urea and guanidinium denaturation curves, *Methods Enzymol. 131*, 266−279.
63. Peoples, R. W., and Weight, F. F. (1995) Cutoff in potency implicates alcohol inhibition of *N*-methyl-D-aspartate receptors in alcohol intoxication, *Proc. Natl. Acad. Sci. U.S.A. 92*, 2825−2829.
64. Nakahiro, M., Arakawa, O., Nishimura, T., and Narahashi, T. (1996) Potentiation of GABA-induced Cl^- current by a series of *n*-alcohols disappears at a cutoff point of a longer-chain *n*-alcohol in rat dorsal root ganglion neurons, *Neurosci. Lett. 205*, 127−130.
65. Shahidullah, M., Harris, T., Germann, M. W., and Covarrubias, M. (2003) Molecular features of an alcohol binding site in a neuronal potassium channel, *Biochemistry 42*, 11243−11252.
66. Myers, J. K., Pace, C. N., and Scholtz, J. M. (1995) Denaturant m values and heat capacity changes: relation to changes in accessible surface areas of protein unfolding, *Protein Sci. 4*, 2138−2148.
67. Pace, C. N., and Shaw, K. L. (2000) Linear extrapolation method of analyzing solvent denaturation curves, *Proteins Suppl. 4*, 1−7.
68. Semisotnov, G. V., Rodionova, N. A., Razgulyaev, O. I., Uversky, V. N., Gripas, A. F., and Gilmanshin, R. I. (1991) Study of the "molten globule" intermediate state in protein folding by a hydrophobic fluorescent probe, *Biopolymers 31*, 119−128.
69. Tcherkasskaya, O., and Uversky, V. N. (2001) Denatured collapsed states in protein folding: example of apomyoglobin, *Proteins 44*, 244−254.
70. Herskovits, T. T., Gadegbeku, B., and Jaillet, H. (1970) On Structural Stability and Solvent Denaturation of Proteins. 1. Denaturation by Alcohols and Glycols, *J. Biol. Chem. 245*, 2588−2598.
71. Avdulov, N. A., Chochina, S. V., Daragan, V. A., Schroeder, F., Mayo, K. H., and Wood, W. G. (1996) Direct binding of ethanol to bovine serum albumin: A fluorescent and C-13 NMR multiplet relaxation study, *35*, 340−347.
72. Wishart, D. S., and Sykes, B. D. (1994) The 13C chemical-shift index: a simple method for the identification of protein secondary structure using 13C chemical-shift data, *J. Biomol. NMR 4*, 171−180.
73. Campanacci, V., Lartigue, A., Hallberg, B. M., Jones, T. A., Giudici-Orticoni, M. T., Tegoni, M., and Cambillau, C. (2003) Moth chernosensory protein exhibits drastic conformational changes and cooperativity on ligand binding, *Proc. Natl. Acad. Sci. U.S.A. 100*, 5069−5074.
74. Briand, L., Nespoulous, C., Huet, J. C., Takahashi, M., and Pernollet, J. C. (2001) Ligand binding and physico-chemical properties of ASP2, a recombinant odorant-binding protein from honeybee (Apis mellifera L.), *Eur. J. Biochem. 268*, 752−760.
75. Kraulis, P. J. (1991) Molscript—a Program to Produce Both Detailed and Schematic Plots of Protein Structures, *J. Appl. Crystallogr. 24*, 946−950.
76. Merritt, E. A., and Bacon, D. J. (1997) Raster3D: Photorealistic molecular graphics, *Methods Enzymol. 277*, 505−524.

BI0516576